



Annals of Glaciology

Supplementary material for

Avoiding slush for hot-point drilling of glacier boreholes

Benjamin H. Hills^{1,2}, Dale P. Winebrenner^{2,1}, W. Timothy Elam^{2,1}, Paul Kintner^{1,2}

¹Department of Earth and Space Sciences, University of Washington, Seattle, WA, USA

²Applied Physics Laboratory, University of Washington, Seattle, WA, USA

Contents:

Text

- S1. Alcohol Properties
- S2. Analytical Solutions
- S3. Two Dimensionality
- S4. Delayed Injection

Tables

- S1. Variables

Figures

- S1. Simulation Time Series
- S2. Freezing-Point Depression
- S3. Enthalpy of Mixing
- S4. Excess Volume
- S5. Viscosity
- S6. Molecular Diffusivity
- S7. Analytical Melt
- S8. Numerical Confirmation – Melting
- S9. Numerical Confirmation – Freezing
- S10. Two Dimensional Simulation
- S11. Injection Timing versus Duration Simulations

Table S1. Variables used in the text.

Variable	Name	Value	Units
ρ_s	Ice Density	917	kg m ⁻³
c_s	Ice Heat Capacity	2097	J kg ⁻¹ °C ⁻¹
k_s	Ice Conductivity	2.1	W m ⁻¹ °C ⁻¹
α_s	Ice Thermal Diffusivity	$\frac{k_s}{\rho_s c_s}$	m ² s ⁻¹
ρ_w	Water Density	1000	kg m ⁻³
c_w	Water Heat Capacity	4212	J kg ⁻¹ °C ⁻¹
k_w	Water Conductivity	.555	W m ⁻¹ °C ⁻¹
α_w	Water Thermal Diffusivity	$\frac{k_w}{\rho_w c_w}$	m ² s ⁻¹
ρ_m	Methanol Density	810	kg m ⁻³
c_m	Methanol Heat Capacity	2400	J kg ⁻¹ °C ⁻¹
k_m	Methanol Conductivity	.203	W m ⁻¹ °C ⁻¹
α_m	Methanol Thermal Diffusivity	$\frac{k_m}{\rho_m c_m}$	m ² s ⁻¹
L	Latent Heat of Fusion	333500	J kg ⁻¹
r	Radial Distance	-	m
R	Phase-Boundary Location	-	m
R_0	Melt Radius	.04	m
r^*	Nondimensionalized Radial Distance	r/R_0	-
R^*	Nondimensionalized Phase Boundary	R/R_0	-
t	Time	-	s
t^*	Nondimensionalized Time	t/t_0	-
t_0	Reference Time (~Time to Freeze Shut)	$\frac{R_0^2 L}{k_s T_\infty }$	-
T_s	Solid Temperature	-	°C
T_l	Liquid Temperature	-	°C
T_∞	Bulk-Ice Temperature	-20	°C
T^*	Nondimensionalized Temperature	T/T_∞	-
Q	Heat Flux from Drill	2500	W
Q^*	Nondimensionalized Heat Flux	$\frac{Q c_s}{4\pi L k_s}$	-
St	Stefan Number	$\frac{c_s (T_f - T_\infty)}{L}$	-
T_f	Freezing Temperature	$T_0 + f(C)$	°C
T_0	Pure Freezing Temperature	0	°C
C	Solution Concentration	-	kg m ⁻³
D	Methanol Molecular Diffusivity	8.4x10 ⁻¹⁰	m ² s ⁻¹
Le	Lewis Number	α/D	-
S	Injection Source through Time	-	kg s ⁻¹
M	Total Injection Mass	-	kg
t_μ	Injection Timing	-	s
σ	Injection Duration	-	s

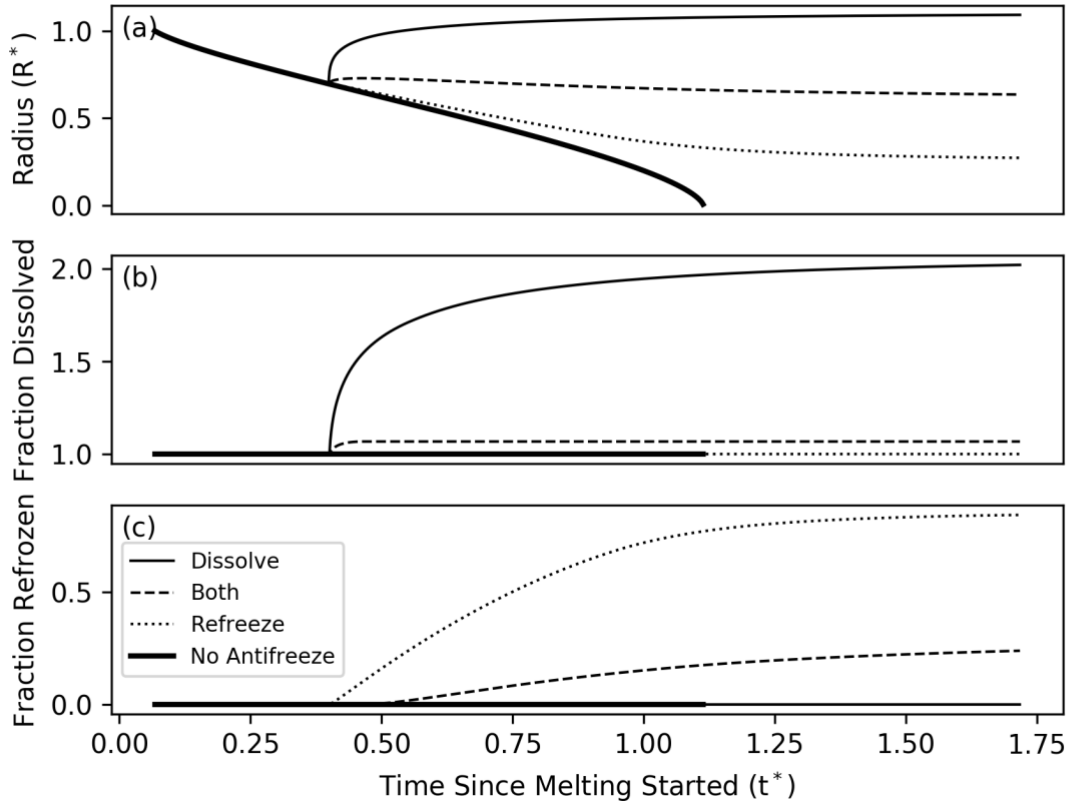


Figure S1. Four selected simulations from the ensemble shown in Figure 2. Here, we show the borehole radius (a), the fraction dissolved (b), and the fraction refrozen (c) through time as the hole evolves. The thick solid line shows the case where no antifreeze is injected and the hole freezes shut. All other cases have some mass of antifreeze injected at $t^* = 0.4$. The thin solid line shows a case where enough antifreeze is injected to dissolve the hole to equilibrium and avoid refreezing entirely ($R_{eq} = 1.1R^*$). The dashed line shows a case where the borehole goes through all four stages described in Figure 1 ($R_{eq} = 0.6R^*$). The dotted line shows a case where the injected antifreeze is insufficient to cause any dissolution, but the borehole continues freezing as slush after the injection ($R_{eq} = 0.25R^*$). The dissolved/refrozen fractions shown here approach equilibrium as the borehole stabilizes (i.e. $t^* \rightarrow \infty$), and those values at equilibrium are equal to the values plotted in Figure 2.

S.1 Alcohol Properties

We assume an aqueous methanol solution for all simulations presented in the manuscript. The physics explored could, however, be translated to any antifreeze solution. As a reference, we note here some of the properties of aqueous methanol and aqueous ethanol solutions, two commonly used antifreeze solutions in ice.

First, freezing-point depression is interpolated between empirical measurements (Flick, 1998) (Fig. S2). The composition at which the solution has the lowest freezing temperature, the eutectic point, is nearly pure alcohol for both cases.

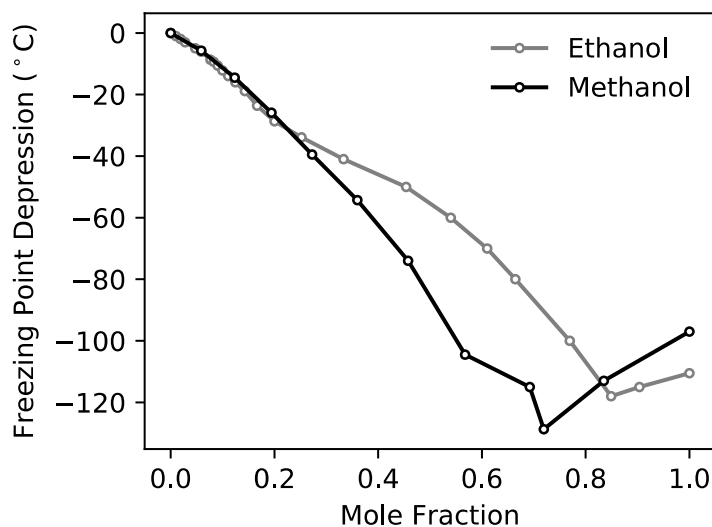


Figure S2. Liquidus line from *Industrial Solvent Handbook* (Flick, 1998). The eutectic point can be seen at ~ 0.85 , -120°C for ethanol and ~ 0.72 , -129°C for methanol.

On mixing of these alcohol solutions, some of the hydrogen bonds in the water molecules are broken, causing the solution to release energy as the exothermic reaction takes place. An empirical relation defines the energy released, termed the 'enthalpy of mixing' (Peeters & Huyskens, 1993) (Fig. S3). Additionally, when the compounds mix there is some excess volume due to the attraction between water and alcohol molecules. The excess volume as a function of mole fraction is shown in Figure S4.

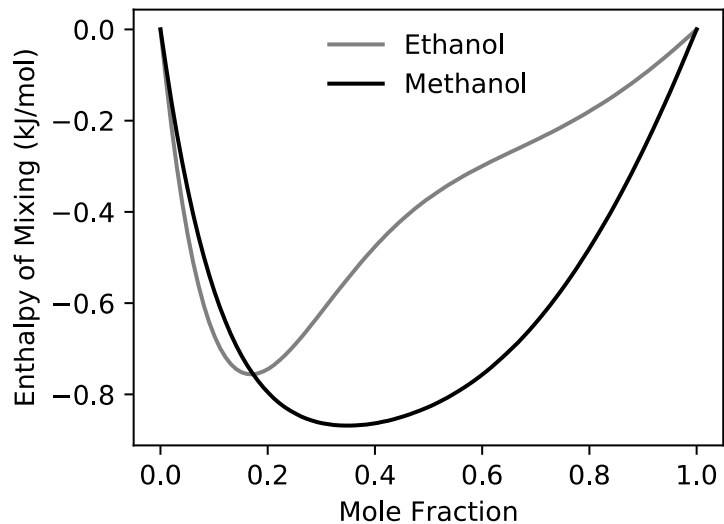


Figure S3. Enthalpy of the exothermic mixing for ethanol/methanol being added to water (Peeters & Huyskens, 1993). Negative enthalpy indicates an exothermic reaction (energy released).

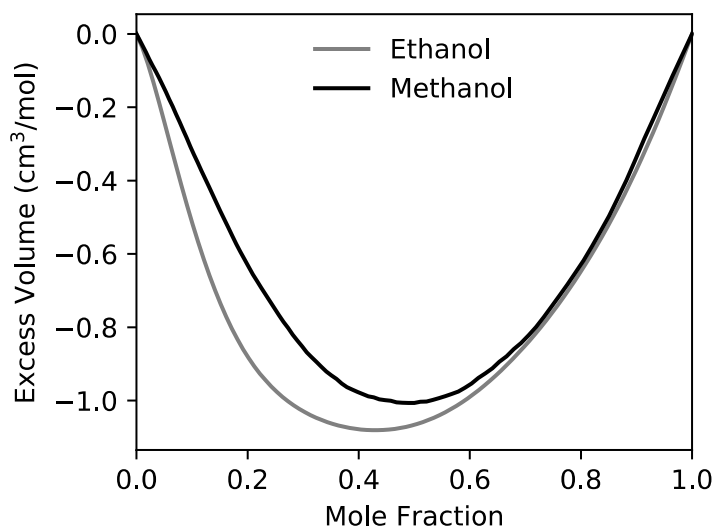


Figure S4. Excess volume of aqueous ethanol/methanol using density data from the Industrial Solvent Handbook (Flick, 1998).

Solution viscosity is plotted for both ethanol and methanol (Fig. S5). Aqueous ethanol viscosity is determined from a Jouyban-Acree model (Khattab et al., 2012). The measurements for this empirical model were taken at considerably warmer temperatures (i.e. 20-50°C), but are extended colder using the Vogel Equation. Aqueous methanol viscosity is linearly interpolated directly from measurements (Yergovich et al., 1971).

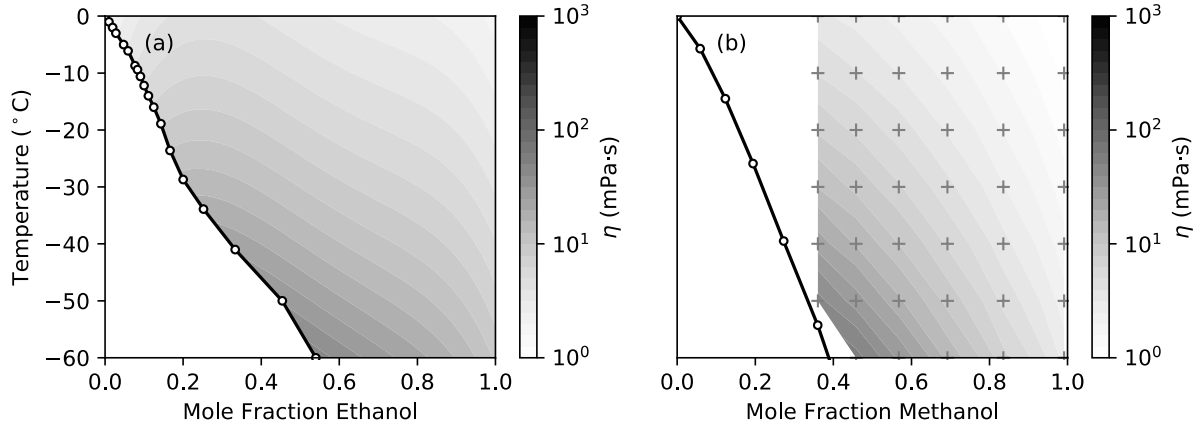


Figure S5. Solution viscosity for aqueous ethanol (a) (Khattab et al., 2012) and methanol (b) (Yergovich et al., 1971). The solid black line with white dots shows the liquidus line for each (as in Fig. S2). For methanol, measurements were taken at the cross locations and viscosity is linearly interpreted from those values.

Molecular diffusivity is the most critical solution property for the slush formation process. As stated in the manuscript, when molecular diffusion is slower than thermal diffusion, molecules accumulate near the borehole wall as it moves inward and force freezing to happen within the solution itself rather than as accretion at the borehole wall. Unfortunately, the molecular diffusivity is also perhaps the most poorly constrained property. In our analysis, we assume a constant value of $8.4 \times 10^{-10} \text{ m}^2 \text{ s}^{-1}$ (Cussler, 1997). However, the true value likely spans about two orders of magnitude depending on the solution temperature and concentration. In Figure S6, we display the range of molecular diffusivities calculated using the Stokes-Einstein equation (Einstein, 1905),

$$D = \frac{k_B T}{6\pi\mu R_p} \quad (\text{S1})$$

where k_B is Boltzmann's constant, T is the solution temperature, μ is the dynamic viscosity (Fig. S5), and R_p is the particle radius. As an upper limit, the reported values are within an order of magnitude of the assumed value above (all significantly lower than the thermal diffusivity). However, the diffusivity could be significantly lower depending on the solution viscosity at low temperatures.

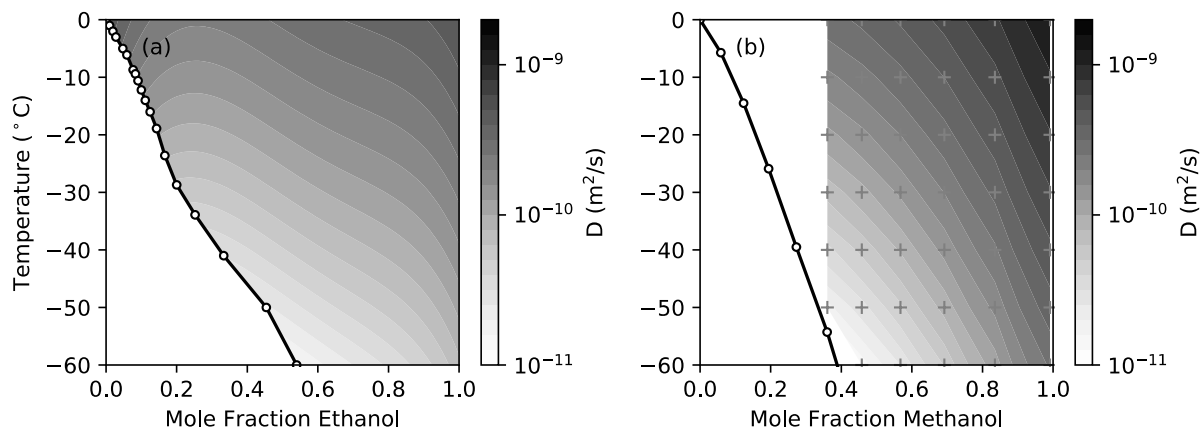


Figure S6. Molecular Diffusivity for aqueous ethanol (a) and aqueous methanol (b) calculated with the Stokes-Einstein equation (eq. S1) using viscosity from Figure S5.

S.2 Analytical Solutions

Considering the cylindrical Stefan problem with a pure solution, some exact analytical solutions exist for the melting case and one approximate solution exists for the freezing case (Crepeau & Siahpush, 2008). Here, we explore these analytical solutions and compare to the numerical solution described in the manuscript.

S.2.1 Melting: Flux at Hole Center

Carslaw and Jaeger (1959; sec. 11.6) pose a problem with a linear heat source at the center of the hole ($r = 0$) and outward melting away from the source. Their problem is solved by thermal evolution around a melting hole as described in the manuscript (i.e. equations 1, and 2). Using their description, the boundary condition at the hole center is

$$\lim_{r \rightarrow 0} 2\pi r k_l \frac{\partial T_l}{\partial r} = Q \quad (S2)$$

where Q is a constant heat flux at the hole center. The conditions at the phase boundary are

$$T_s(R, t) = T_l(R, t) = T_f \quad (S3)$$

$$\rho_s L \frac{dR}{dt} = k_s \left. \frac{\partial T_s}{\partial r} \right|_R - k_l \left. \frac{\partial T_l}{\partial r} \right|_R \quad (S4)$$

where T_f is a constant freezing temperature. Finally, the bulk-ice temperature is

$$T_s \rightarrow T_\infty, \quad \text{as } r \rightarrow \infty \quad (S5)$$

Following the solution laid out in Carslaw and Jaegar (1959; sec. 11.6), we assume solutions of the form

$$-Ei(-\gamma^2) \quad (S6)$$

where the nondimensional radius is

$$\gamma = \frac{r}{2\sqrt{\alpha t}} \quad (S7)$$

and $Ei(\)$ is an exponential integral. Then, at the phase boundary,

$$R = 2\lambda\sqrt{\alpha_s t} \quad (S8)$$

Now, we solve for the temperature profiles, first in the liquid. Taking the form (S6), the liquid temperature is

$$T_l = A_1 - B_1 \left(Ei(-\gamma_l^2) \right) \quad (S9)$$

Plugging in the relevant boundary conditions (equations S2, S3, and S8) gives the solution

$$T_l = T_f + \frac{Q}{4\pi k_l} \left(Ei(-\gamma_l^2) - Ei\left(-\lambda^2 \frac{\alpha_s}{\alpha_l}\right) \right) \quad (S10)$$

Now, similarly for the solid,

$$T_s = A_2 - B_2(Ei(-\gamma_s^2)) \quad (S11)$$

and boundary conditions (equations S3, S5, and S8) gives

$$T_s = T_\infty + \frac{(T_f - T_\infty)}{Ei(-\lambda^2)} Ei(-\gamma_s^2) \quad (S12)$$

Finally, solve for the transcendental equation using the Stefan condition (equation S4)

$$\begin{aligned} \rho_s L \frac{\partial}{\partial t} (2\lambda \sqrt{\alpha_s t}) \\ = k_s \frac{\partial}{\partial r} \Big|_R (T_\infty - A_2 Ei(-\gamma_s^2)) \\ - k_l \frac{\partial}{\partial r} \Big|_R \left(T_f + A_1 \left(Ei(-\gamma_l^2) - Ei\left(-\lambda^2 \frac{\alpha_s}{\alpha_l}\right) \right) \right) \end{aligned} \quad (S13)$$

Plugging in the solutions above

$$\frac{Q}{4\pi} e^{-\lambda^2 \frac{\alpha_s}{\alpha_l}} + \frac{k_s (T_f - T_\infty)}{Ei(-\lambda^2)} e^{-\lambda^2} = \lambda^2 \alpha_s L \rho_s \quad (S14)$$

and nondimensionalized gives

$$Q^* e^{-\lambda^2 \frac{\alpha_s}{\alpha_l}} + \frac{St}{Ei(-\lambda^2)} e^{-\lambda^2} = \lambda^2 \quad (S15)$$

with a non-dimensional heat flux

$$Q^* = \frac{Q c_s}{4\pi L k_s} \quad (S16)$$

and the Stefan number,

$$St = \frac{c_s (T_f - T_\infty)}{L} \quad (S17)$$

Using this solution (equation S15), we can assess the energy necessary to melt out a glacier borehole, or even to keep the hole open after drilling, using a linear source in the hole. While melting out the hole with this type of fixed source is likely impractical due to the energy constraints (Suto et al., 2008), keeping the hole open for a short period of time is more plausible. In fact, in locations where environmental regulations will restrict antifreeze usage (such as near the ice-sheet bed) using a line source may be a legitimate alternative.

S.2.2 Melting: Flux at Hole Wall

Instead of the hole-centered heat flux described above, the most appropriate solution for the hot-point drilling case is that in which a heat flux follows the motion of the phase-transition boundary. That is, as the hole melts out the drill moves downward, continuously in contact with the ice and progressively melting the hole. The analytical solution for this case is derived from a slightly simplified form of the above equations, considering heat transport within the ice only, and with a boundary condition at the moving phase boundary, $r = R$,

$$k_l \frac{\partial T(R, t)}{\partial r} = -\frac{Q}{2\pi R} \quad (\text{S18})$$

Substituting, the Stefan condition is then

$$k_s \frac{\partial T(R, t)}{\partial r} + \frac{Q}{2\pi R} = \rho_s L \frac{\partial R}{\partial t} \quad (\text{S19})$$

The temperature solution is the same as above, but with the hole wall progressing at a slightly different rate determined by the transcendental equation,

$$\frac{St}{Ei(-\lambda^2)} e^{-\lambda^2} + Q^* = \lambda^2 \quad (\text{S20})$$

This solution (equation S20) shows that the hole will melt faster here than in the hole-centered heat flux case (equation S15) (Figure S7). We test the numerical model described in the manuscript against this analytical solution, showing that the resulting temperature profiles and rate of borehole melting are identical (Figure S8).

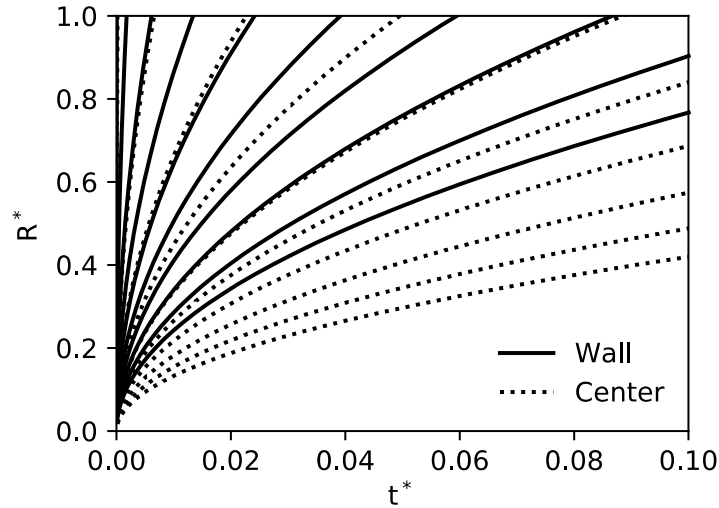


Figure S7. The analytic solution of the borehole wall location for constant Q^* and variable St (i.e. 0.25, 0.18, 0.13, 0.06, 0.03, 0.006) for flux at the hole wall (solid) and flux at the center of the hole (dotted).

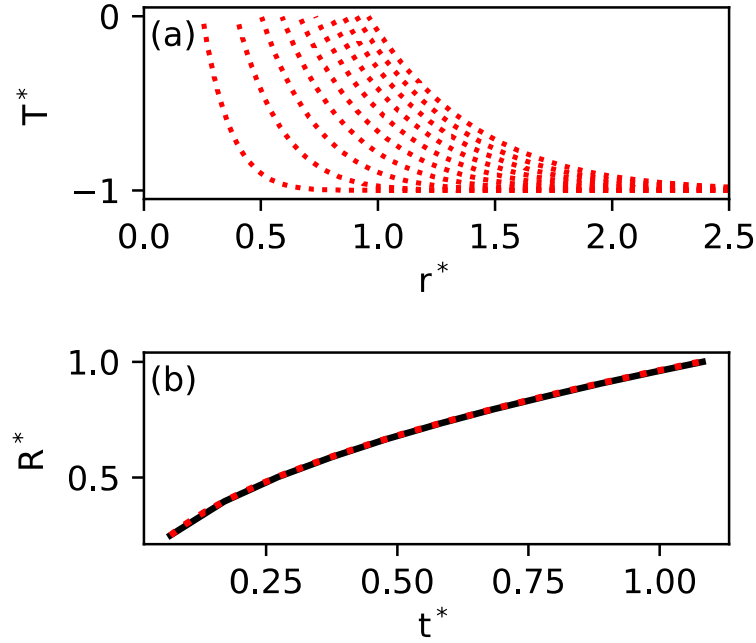


Figure S8. A comparison of numerical (red dotted) and analytical (black solid) for the case of melt out to 0.04 m with constant flux at the hole wall, $Q = 2.5\text{kW/m}$, $T_0 = -20^\circ\text{C}$.

S.2.3 Approximate Freezing Solution

Following (Crepeau & Siahpush, 2008) there is an approximate analytical solution for a hole freezing shut if the domain is finite and the outer boundary condition is fixed to some constant temperature. Boundary conditions in this case are

$$T = T_0, \quad r = r_0 \quad (\text{S21})$$

$$\frac{\partial T}{\partial r} = 0, \quad r = 0 \quad (\text{S22})$$

$$T = T_f, \quad r = R \quad (\text{S23})$$

where r_0 is the extent of the domain. Their solution is

$$T_l = \frac{\dot{q}R^2}{4k_l} \left(1 - \frac{r^2}{R^2} \right) + T_f \quad (\text{S24})$$

$$T_s = \frac{-\dot{q}r^2}{4k_s} \frac{(R^2 \ln(r_0) - r_0^2 \ln(R) + (R^2 - r_0^2) \ln(R))\dot{q} + 4k_s(T_f \ln(r_0) - T_0 \ln(R) + (T_f - T_0) \ln(r))}{4k_s \ln\left(\frac{R}{r_0}\right)} \quad (\text{S25})$$

where \dot{q} is a heat source throughout the domain. The interface location is then defined by a differential equation

$$\rho_i L \frac{dR}{dt} = \frac{(R^2 - r_0^2)\dot{q} + 4k_i(T_f - T_0)}{4R \left(\ln\left(\frac{R}{r_0}\right)\right)} \quad (\text{S26})$$

Note that this solution is approximate. Crepeau and Siahpush (2008) assume thermodynamic equilibrium within the solution, and they consider only cases with some positive heat source so that the solution converges onto a steady temperature profile with the hole remaining open. With the limitations of this approximate solution in mind, we plot temperature profiles and the associated phase boundary location for the case of no internal heat source, thus allowing the hole to completely freeze shut and again compare this to our numerical solution from the manuscript (Figure S9).

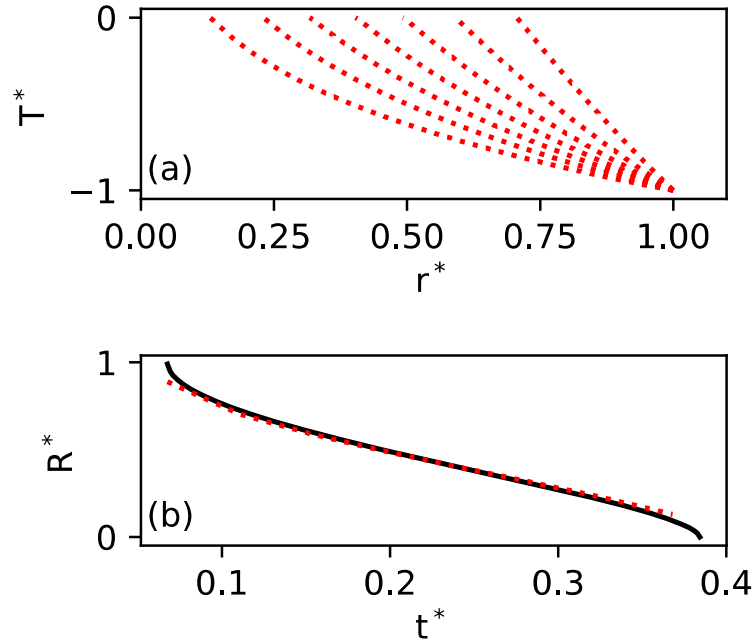


Figure S9. The approximate solution for borehole freezing shut (Crepeau & Siahpush, 2008) with no internal heating, $\dot{q} = 0$.

S.3 Two Dimensionality

Up to now, we have treated the system as one-dimensional. In reality, the drill moves downward and warms the surrounding ice as it moves. Radial symmetry means that the problem can at least be reduced to two dimensions (z and r), but here we want to test whether our original assumption to neglect the vertical advection and diffusion is valid.

In two dimensions, again in cylindrical coordinates and with the logarithmic transformation, the heat equation is

$$\frac{\partial T}{\partial t} = \nabla \cdot (\alpha_s \nabla T) - u_z \frac{\partial T}{\partial z} \quad (\text{S27})$$

with the vertical velocity, u_z , being prescribed by the drilling rate. This is a Lagrangian framework, where the mesh moves with the drill and the ice (which is not moving in the Eulerian sense) now moves up and out of the domain. To test the two-dimensionality of the problem we create a drill-like scenario with boundary conditions fixed to the bulk ice temperature below the drill and as $r \rightarrow \infty$, the ice temperature to the melting point at $r = 0$, and zero flux at the top of the domain.

At the limit where $u_z \rightarrow 0$ or where $z \rightarrow \infty$, the above problem reduces to one dimension as in our original simulations. Our question though, is how slow the drill rate needs to be or how far behind the drill we need to look for this to be the case. Results for the two-dimensional case with drilling rate, $u_z = 2 \text{ m/hr}$, and the bulk-ice temperature, $T_\infty = -20^\circ\text{C}$, and are shown in Figure S10. Here, we confirm that the zero velocity case is indeed one-dimensional. Interestingly, we also see that the nonzero case perfectly matches the one dimensional solution for some time (i.e. the first few hours in Fig. S10b) and then approaches a steady state. Additionally, the two-dimensional model converges to the one-dimensional result with increasing vertical distance behind the drill (Fig. S10c). Based on these results we assert that at short timescales (hours) or far distances behind the drill (~ 500 times the borehole radius in this case) the problem is exactly one-dimensional.

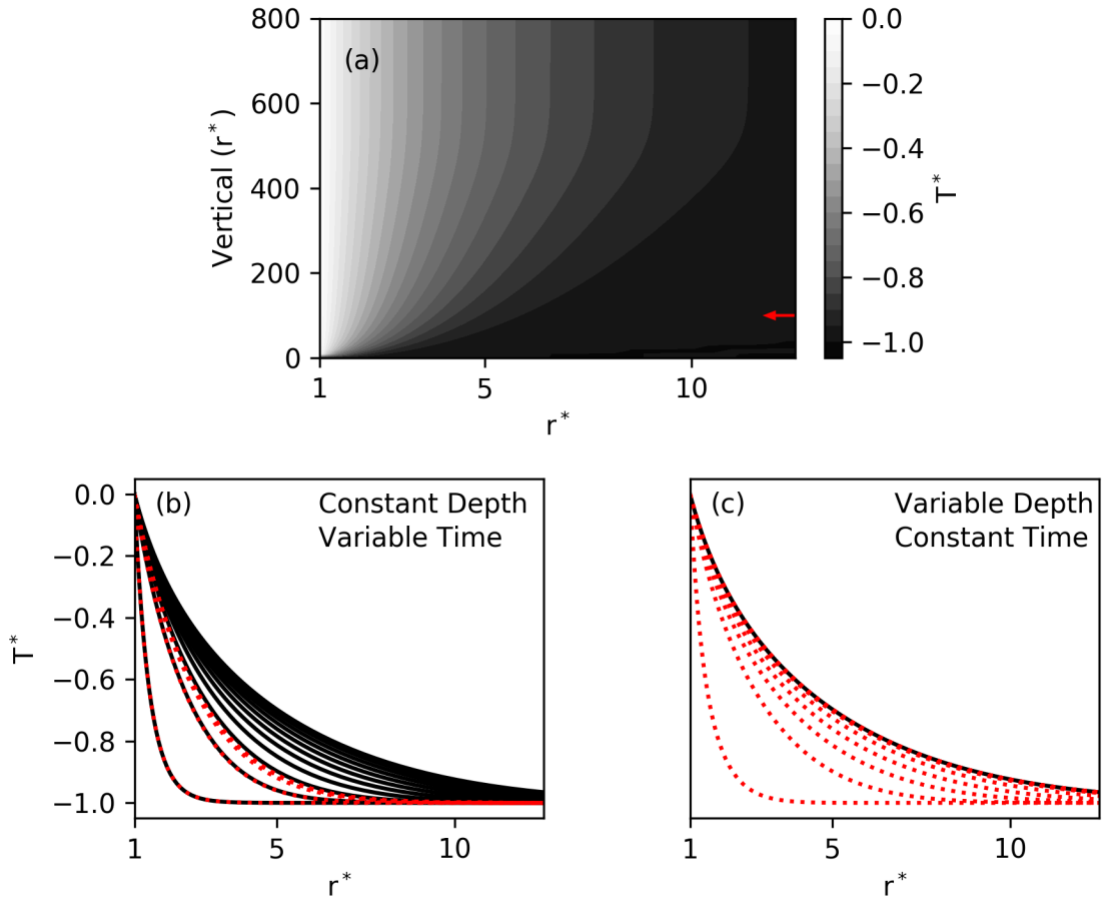


Figure S10. a) The temperature result for the 2-dimensional case of drilling at 2 m/hr with the model run for 10 hours. The hypothetical 'drill tip' is at (1,0). b) Temperature profiles at hourly time steps over the 10-hour simulation. The 1-D model is shown in black, and the 2-D model (red dotted) corresponds to a location 5 m above the drill tip (red arrow in (a)). c) Temperature profiles at the end of the 10-hour simulation at depth increments of $100r^*$ from bottom to top of the 2-dimensional domain in (a) (red dotted). For comparison, the 1-dimensional result at the end of a 10-hour simulation is shown in black.

S.4 Delayed Injection

As discussed in the manuscript, refreezing can be minimized by slowing the rate of injection (Humphrey & Echelmeyer, 1990 Fig. 13). Here, we quantify this effect using an ensemble of simulations with varying injection timing and injection duration. For each simulation, the antifreeze source is described as a Gaussian function through time

$$S(t) = \frac{M}{\sigma\sqrt{2\pi}} e^{-\frac{1}{2}\left(\frac{t-t_\mu}{\sigma}\right)^2} \quad (\text{S28})$$

where M is the total mass of injected antifreeze, σ is the injection duration, and t_μ is the injection timing. For every simulation, the total mass of injected antifreeze (i.e. the integrated source) is exactly enough to stabilize the hole to the size at the time of injection (following the reference ‘radius at injection’ line in Figure 2). As expected, the results show less refreezing with a more prolonged injection (Fig. S11).

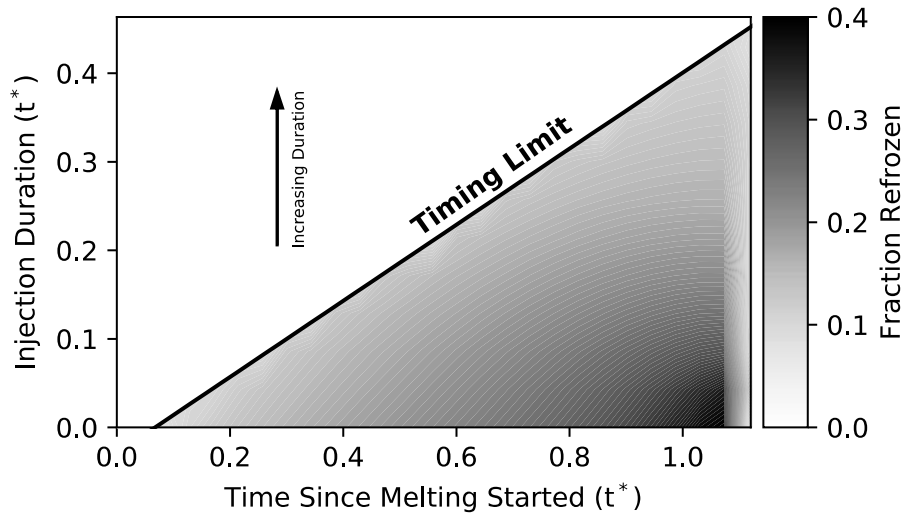


Figure S11. Model results for an ensemble of simulations with variable injection timing and injection duration. For these simulations, the total mass of injected antifreeze is always the exact amount necessary to stabilize the borehole to the radius at the time of injection (black in Figure 2). Fraction refrozen is calculated as in Figure 2. The timing limit (black) shows the cutoff for plausible simulations (i.e. any simulation with earlier injection timing or a longer injection duration would require some injection before the hole starts freezing shut).

References

- Carslaw, H. S., & Jaeger, J. C. (1959). *Conduction of Heat in Solids* (Second). London: Oxford University Press.
- Crepeau, J., & Siahpush, A. (2008). Analytical solutions to the Stefan problem with internal heat generation. *Heat and Mass Transfer*, *44*, 787–794. <https://doi.org/10.1016/j.applthermaleng.2016.03.122>
- Cussler, E. L. (1997). *Diffusion: Mass Transfer in Fluid Systems*. Cambridge, UK: Cambridge University Press.
- Einstein, A. (1905). Über die von der molekularkinetischen Theorie der Wärme geforderte Bewegung von in ruhenden Flüssigkeiten suspendierten Teilchen. *Annalen Der Physik*, *322*(8), 549–560.
- Flick, E. W. (1998). *Industrial Solvents Handbook* (5th ed.). Westwood, NJ: Noyes Data Corporation.
- Humphrey, N., & Echelmeyer, K. (1990). Hot-water drilling and bore-hole closure in cold ice. *Journal of Glaciology*, *36*(124), 287–298. <https://doi.org/10.3189/002214390793701354>
- Khattab, I. S., Bandarkar, F., Fakhree, M. A. A., & Jouyban, A. (2012). Density, viscosity, and surface tension of water+ethanol mixtures from 293 to 323K. *Korean Journal of Chemical Engineering*, *29*(6), 812–817. <https://doi.org/10.1007/s11814-011-0239-6>
- Peeters, D., & Huyskens, P. (1993). Endothermicity or exothermicity of water/alcohol mixtures. *Journal of Molecular Structure*, *300*(C), 539–550. [https://doi.org/10.1016/0022-2860\(93\)87046-C](https://doi.org/10.1016/0022-2860(93)87046-C)
- Suto, Y., Saito, S., Osada, K. ichi, Takahashi, H., Motoyama, H., Fujii, Y., & Tanaka, Y. (2008). Laboratory experiments and thermal calculations for the development of a next-generation glacier-ice exploration system: Development of an electro-thermal drilling device. *Polar Science*, *2*(1), 15–26. <https://doi.org/10.1016/j.polar.2008.02.002>
- Yergovich, T. W., Swift, G. W., & Kurata, F. (1971). Density and viscosity of aqueous solutions of methanol and acetone from the freezing point to 10°C. *Journal of Chemical and Engineering Data*, *16*(2), 222–226.